Optics Letters

Quasi-phase matched second harmonic generation in a PMN-38PT crystal

Xin Chen,[1,†] Leszek Mateusz Mazur,[2,3,†] Dawei Liu,[4] Shan Liu,[4] Xin Liu,[5] Zhuo Xu,[5] Xiaoyong Wei,[5] Junli Wang,[1,8] Yan Sheng,[4,6,9] Zhiyi Wei,[7] and Wieslaw Krolikowski[2,4]

[1]School of Physics, Xidian University, Xi'an 710071, China
[2]Science Program, Texas A&M University at Qatar, Doha 23874, Qatar
[3]Advanced Materials Engineering and Modelling Group, Faculty of Chemistry, Wroclaw University of Science and Technology, Wyb. Wyspianskiego 27, 50-370 Wroclaw, Poland
[4]Laser Physics Centre, Research School of Physics, Australian National University, Canberra, ACT 0200, Australia
[5]Electronic Materials Research Laboratory, Key Laboratory of the Ministry of Education and International Center for Dielectric Research, Xi'an Jiaotong University, Xi'an 710049, China
[6]Laboratory of Infrared Materials and Devices, Research Institute of Advanced Technologies, Ningbo University Ningbo, Zhejiang 315211, China
[7]Beijing National Laboratory for Condensed Matter Physics, Institute of Physics, Chinese Academy of Sciences, Beijing 100190, China
[8]e-mail: dispersion@126.com
[9]e-mail: yan.sheng@anu.edu.au
[†]These authors contributed equally to this Letter.

Received 30 November 2021; revised 10 March 2022; accepted 15 March 2022; posted 16 March 2022; published 13 April 2022

We used an all-optical poling method to fabricate quadratic nonlinearity gratings in a tetragonal $0.62Pb(Mg_{1/3}Nb_{2/3})O_3$-$0.38PbTiO_3$ (PMN-38PT) crystal. We then employed these gratings in quasi-phase matched collinear second harmonic generation processes. By measuring the second harmonic output, we provided, for the first time, to the best of our knowledge, quantitative estimates of all three non-zero quadratic nonlinearity coefficients of the PMN-38PT crystal.

https://doi.org/10.1364/OL.450042

There has been continuous interest in PT-relaxor ferroelectrics due to their excellent physical properties [1,2]. Giant piezoelectric constants [3,4], high acoustics [5], and electro-optic constants [6] make these materials excellent candidates for application in monolithic phononic crystals. Furthermore, thanks to the lack of center of inversion, these materials exhibit second-order (quadratic) nonlinear properties. A combination of phononic, electro-optic, and optical nonlinear properties in those materials would make them invaluable in fabricating integrated, nonlinear acousto-optic devices. However, it appears that many of the PT-relaxors have not been studied in the context of their optical nonlinearity. Recent work with powdered $Pb(Mg_{1/3}Nb_{2/3})O_3$-$PbTiO_3$ (PMN-PT) crystals indicated promising second-order nonlinear properties, which could be used in frequency conversion [7]. However, the efficiency of frequency conversion is often hindered by the dispersion-caused mismatch between phases of the nonlinear polarization and that of generated new wave(s). Taking second harmonic generation (SHG) as an example, the phase mismatch $\Delta k = k_2 - 2k_1$, where $k_1 = 2\pi n_\omega/\lambda_1$ and $k_2 = 2\pi n_{2\omega}/\lambda_2$ are the wave vectors of the fundamental beam (FB) and second harmonic (SH), and n_ω, λ_1 and $n_{2\omega}$, λ_2 are refractive indices and wavelengths of the FB and SH, respectively. To achieve phase matching and ensure efficient interaction, one may make use of the birefringence of the nonlinear crystal. This so-called birefringent phase matching involves appropriate choice of polarization of the interacting waves [8], their propagation direction, and the temperature of the crystal. For instance, in the transmission window (0.45–5.5 μm) of a tetragonal $0.62Pb(Mg_{1/3}Nb_{2/3})O_3$-$0.38PbTiO_3$ (PMN-38PT) crystal at room temperature, the birefringent phase matching can only be realized in the mid-infrared at $\lambda_1 = 3.261$ μm or $\lambda_1 = 4.598$ μm, depending on the type of nonlinear interaction.

An alternative and more flexible approach involves spatial periodic modulation of the quadratic nonlinear susceptibility tensor $\chi^{(2)}$, which ensures that the relative phase between interacting waves is always less than π. Therefore, the energy keeps flowing from the FB to the SH. This is the so-called quasi-phase matching (QPM) technique [9,10]. In ferroelectrics, spatial nonlinearity modulation is realized by creating periodic ferroelectric domain structures through patterned electrodes biased with high external voltage along a crystal's polar axis [11]. Unfortunately, electric field poling in PMN-PT crystals remains challenging. These crystals are prone to cracking due to the large strain induced by the electric field [12]. In addition, undesired 90° domains can be formed during electrical poling [13,14]. Other methods, e.g., electron beam poling, are not practical for fabricating QPM structures due to the limited depth of the inverted domains [15]. Significant progress was achieved very recently, in which 3D domain inversion was realized in PMN-PT crystals with the femtosecond laser poling technique [16]. However,

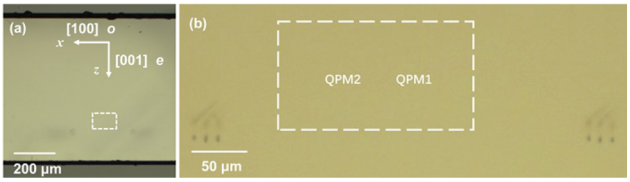

Fig. 1. (a) Front view of the PMN-38PT sample. The 3.4 mm (x) × 2.4 mm (y) × 0.7 mm (z) crystal was supported by glass plates to simplify its handling. The input polarization of the FB along the z ([001]) and x ([100]) axes is denoted as e (extraordinary) and o (ordinary), respectively. The location of both QPM gratings is indicated by white rectangular box. (b) Magnified section of the sample with main QPM gratings. Permanent damages (black spots) are induced for easy alignment.

those structures were restricted to very limited areas. Subsequently, to the best of our knowledge, QPM interaction has never been demonstrated in PMN-PT crystals.

In this work, we study experimentally SHG in PMN-38PT crystals. To this end, we create periodic ferroelectric domain structures (nonlinear gratings) in the crystal via the laser poling technique [17–21], and demonstrate collinear quasi-phase matched SHG. Using the measured output power of the SH signal, we were able to determine the relative strengths of the $\chi^{(2)}$ coefficients in this crystal as well as provide a quantitative estimate of their values. This work constitutes the first ever quantitative measurement of the quadratic nonlinearity in the PMN-PT crystal. Our results open the possibility to develop a class of hybrid devices combining the excellent piezoelectric and optical properties of relaxor-based ferroelectric crystals.

We used PMN-38PT crystals grown via a modified Bridgman technique [22]. The [001] direction of the single crystal was oriented by using the rotating orientation x ray diffraction method [23]. The bulk single crystal was then diced into small plates, cutting perpendicular to the [001] direction (z-cut) with side cuts parallel to the (010) and (100) planes. All facets of the plates were polished to optical grade. To fabricate single-domain PMN-38PT crystals without cracking, a thermal annealing treatment, followed by a high-temperature poling process, was applied [16]. Figure 1 shows the front view (xoz) of the mounted sample. The fact that the nonlinear gratings themselves are all but invisible serves as a proof that our optical writing process involves domain reversal without distorting the crystalline structure.

In this work, we realized the $\chi^{(2)}$ modulation by laser-induced ferroelectric domain inversion. In this approach, an infrared short pulse beam tightly focused inside the crystal with its energy below the damage threshold (here less than 0.12 J/cm^2) locally flips its spontaneous polarization [16,19–21]. We used a femtosecond oscillator (MIRA, Coherent) to generate laser pulses with a wavelength of 800 nm, pulse duration of 180 fs, and repetition rate of 80 MHz. The pulse energy of the laser beam can be continuously adjusted from 0 nJ to 5 nJ by utilizing a half-wave plate followed by a polarizer. The laser beam was then focused into the monodomain PMN-PT crystal by a ×20 microscope objective (NA = 0.4). The sample was mounted on an xyz-translation stage with stepper motor actuators. With a combination of the stage and an optical shutter, 3D ferroelectric domain structures could be inscribed, starting from 200 μm beneath the $+z$ surface, and moving deeper inside the crystal. By using 1 micron or less spatial separation between individual laser beam spots, the inverted domains merged, forming

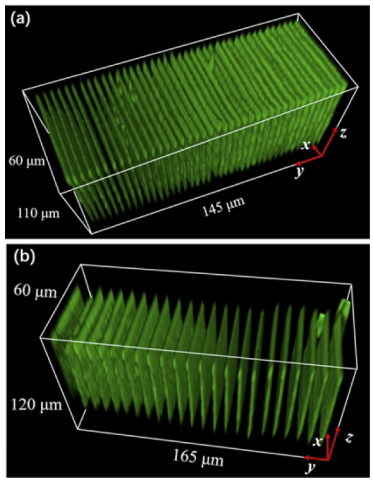

Fig. 2. Nonlinear microscopy images of the fabricated periodic, inverted domain structures. The grey planes represent regions of inverted spontaneous polarization. (a) Domain structure QPM1, with period of 3.5 μm and total length of 2 mm. (b) Domain structure QPM2 with period of 7.1 μm and total length of 1.13 mm.

rectangular (45 μm × 100 μm) stripes in the xoz plane. We fabricated two periodic domain structures with different periods and lengths. The first one (QPM1) is 2 mm long with a period of 3.5 μm, and the second one (QPM2) is 1.13 mm long with a period of 7.1 μm. The periods of both structures were chosen such that they could operate in the quasi-phase matched regime at central wavelengths of 1037 nm and 1254 nm for QPM1 and QPM2, respectively. The periodic domain structures were visualized using nonlinear Čerenkov microscopy, which is sensitive to abrupt changes of $\chi^{(2)}$ nonlinearity [24]. Both nonlinear structures are depicted in Fig. 2.

We measured the intrinsic optical losses introduced by the QPM structures by comparing the transmission of a weak light beam through the grating region with that of pristine crystal. The losses were less than 0.1 dB/cm at 1260 nm. This confirms that the laser poling did not introduce any amorphization of the material, which typically leads to strong light scattering [25].

In the SHG experiments, the FB was delivered by the Coherent Chameleon Ultra II+ compact c-OPO system with a pulse duration of 200 fs and repetition rate of 80 MHz. The linearly polarized FB was focused onto the structure (xoz plane) with either 45 mm or 25 mm focal length lens, and propagated along the y direction. The corresponding beam widths (at the e^{-2} level) were 24 μm and 16 μm, respectively. The wavelength of the FB was tunable in the range of 1000–1600 nm. The input polarization could be rotated to coincide with ordinary [100], extraordinary [001], or mixed [101] directions. The average power of the SH ($P_{2\omega}$) was recorded at the exit of the sample. The average power of the FB (P_{ω}) was kept constant at 100 mW. As the PMN-38PT crystal belongs to the 4 mm symmetry group, the $\chi^{(2)}$ tensor has only three non-zero elements (d_{31}, d_{33}, and d_{15}). Thus, three different SHG processes are possible, depending on the polarization of the FB and SH. Denoting ordinary and extraordinary polarization by "o" and "e," respectively, these interactions are $ee \rightarrow e$ (mediated via the d_{33} coefficient), $oe \rightarrow o$ (mediated via the d_{15} coefficient), and $oo \rightarrow e$ (mediated via the d_{31} coefficient). For instance, for the $oe \rightarrow o$ interaction, in which one ordinary and one extraordinary

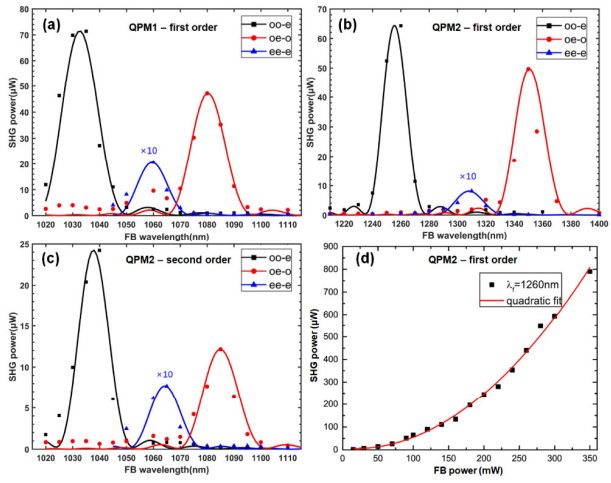

Fig. 3. Quasi-phase-matched SHGs in the PMN-38PT crystal. Output SH power as a function of the wavelength and polarization of the FB for (a) QPM1 and (b), (c) QPM2. The curves represent the $\sin^2(\Delta k l_e/2)/(\Delta k l_e/2)^2$ fit with $l_e = 0.7 l_t$. The input beam diameter was 16 μm in (a) and (c) and 24 μm in (b). (d) Output SH power versus input power generated in QPM2. The input power of the FB was set at 100 mW in (a)–(c).

fundamental photon combine creating a single, ordinarily polarized photon at doubled frequency, the phase matching condition reads: $\Delta k = k_{1e} + k_{1o} - k_{2o} + mQ = 0$. Here, k_{1e} and k_{1o} are wave vectors of the extraordinary and ordinary polarized components of the FB, while k_{2o} is the wave vector of the SH emitted with ordinary polarization; $Q = 2\pi/\Lambda$ represents the basic reciprocal vector of the nonlinearity modulation with period Λ, while m is an integer indicating the order of the nonlinear interaction.

Figures 3(a)–3(c) depict the measured power (its ordinary and extraordinary components) of the SHG in each structure, as a function of the wavelength and polarization state of the input FB. The bell-shaped tuning curves in each graph correspond to three different nonlinear interaction processes, and each SH peak reflects the relevant QPM resonance. The plots in Figs. 3(a) and 3(b) represent the first-order ($m = 1$) nonlinear interaction in QPM1 and QPM2, respectively. The graph in Fig. 3(c) depicts the second-order nonlinear interaction ($m = 2$) in QPM2. As the period in QPM2 is roughly two times longer than that of QPM1, the resonance peaks in the second-order interaction in the former structure are very close to those measured in the first-order interaction in the latter. For completeness, the graph in Fig. 3(d) depicts $P_{2\omega}$ in QPM2 as a function of P_{ω}. As expected, the quadratic relation is evident.

The tuning curves in Figs. 3(a)–3(c) were obtained by fitting the $\sin^2(\Delta k l_e/2)/(\Delta k l_e/2)^2$ function to the experimental data. The fitting parameter l_e represents the effective interaction length determined by two factors, namely the walk-off length and spectral width of the input pulse. The former, $l_t = \tau/[v_g^{-1}(2\omega) - v_g^{-1}(\omega)]$, with τ being the pulse length, represents the difference between group velocities of the FB ($v_g(\omega)$) and SH ($v_g(2\omega)$), and consequently defines the region of coherent interaction between both waves. Together with the spectral width of the input pulse they contribute to the broadening of the tuning curves. The broadening may further increase by fabrication errors in the nonlinearity pattern [26].

We will use the experimental results to estimate the nonlinear coefficients using the following formula for $P_{2\omega}$ in the short pulse regime at resonance [27]:

$$P_{2\omega} = \frac{16\pi^2 d_{eff}^2 P_{\omega}^2 l_t t_{rep}}{n_{\omega} n_{2\omega} c \varepsilon_0 \lambda_1^3 \tau} \frac{L}{b}, \tag{1}$$

where d_{eff} is the effective nonlinear coefficient, t_{rep} is the repetition period, L is the length of the periodic structure, c is the speed of light, ε_0 is the vacuum permittivity, τ is the pulse length, b is the confocal parameter of the input beam, and n_{ω} and $n_{2\omega}$ are refractive indices of the FB and SH, respectively. The walk-off length l_t and refractive indices were evaluated from the Sellmeier formula for the PMN-38PT crystal [28]. For the $oo \rightarrow e$ resonance, $l_t = 105$ μm and 185 μm at 1035 nm and 1260 nm, respectively.

The effective nonlinear coefficient d_{eff} depends on the element of the $\chi^{(2)}$ tensor, the duty cycle of the nonlinearity modulation (D), and the order (m) of the nonlinear interaction [29]. For the *oo-e* interaction, d_{eff} has the following form:

$$d_{eff} = \frac{2 d_{31}}{\pi m} \sin(\pi m D). \tag{2}$$

The duty cycle in our laser-fabricated structures was close to 0.5 in the case of QPM1 and 0.25 for QPM2, respectively. It is clear from Eq. (2) that duty cycle $D = 0.5$ corresponds to the strongest effective nonlinearity. In an optically poled domain structure, the duty cycle could be adjusted by carefully controlling the domain width within the poling period. For instance, the domain width can be adjusted by changing the numerical aperture of the laser beam focusing lens. In addition, in an optically poled domain structure with relatively large poling period, the duty cycle can be increased by inscribing closely two or more groups of domains, so they can merge, thereby forming much thicker objects.

The experimental results are summarized in Table 1, which depicts the $P_{2\omega}$ recorded at each QPM resonance. By comparing $P_{2\omega}$ in all interaction regimes, one can determine the relative magnitudes of all nonlinear coefficients. We found that d_{15}, d_{31}, and d_{33} satisfy the following relations: $|d_{15}| \approx 0.4|d_{31}|$ and $|d_{33}| \approx 0.17|d_{31}|$. These values are expected to be rather accurate, as they involve the power ratios measured in the same experimental conditions. A more careful approach is needed while using Eq. (1) to find an absolute value of the nonlinear coefficients, as the result may be strongly affected by the uncertainty of the parameters of the laser beam. When using Eq. (1), we find an

Table 1. Experimental Parameters and Results of Quasi-Phase Matched SHs in the QPM Structures, Where *m* Is the Interaction Order, *f* Is the Focal Length, and $P_{2\omega}$ Is the Average Power of the SH

Structure	m	f (mm)	*ee-e* (via d_{33})		*oe-o* (via d_{15})		*oo-e* (via d_{31})	
			$P_{2\omega}$ (μW)	λ_1 (nm)	$P_{2\omega}$ (μW)	λ_1 (nm)	$P_{2\omega}$ (μW)	λ_1 (nm)
QPM1	1	45	2.06	1060	47.16	1080	71.38	1035
QPM2	1	25	0.81	1310	49.67	1350	64.31	1260
QPM2	2	45	0.77	1065	12.16	1085	24.22	1040

average value of the nonlinear coefficient as $d_{31} \approx 1.3$ pm/V. To corroborate this result, we conducted a control experiment in a calcium barium niobate ($Ca_{0.28}Ba_{0.72}Nb_2O_6$, CBN) crystal, whose nonlinearity and refractive indices (via the Sellmeier formula) are known [30,31]. To this end we optically fabricated a 100-μm-long nonlinear grating with period of 8.8 μm and duty cycle of 0.35 in the CBN sample. Then, using the same focusing conditions as in the PMN-38PT crystal case, we realized the quasi-phase matched SHG via $ee \rightarrow e$ interaction at 1170 nm. Using the measured $P_{2\omega}$ in Eq. (1) gives $d_{33}^{(CBN)} \approx 7.0$ pm/V. This agrees reasonably well with the reported earlier value of 9 (±2) pm/V [30] and, hence, confirms the validity of our PMN-38PT crystal results.

In conclusion, we demonstrated experimentally, for the first time, quasi-phase matched, collinear SHG in a ferroelectric PMN-38PT crystal. By varying the input linear polarization, we observed three nonlinear interaction processes. The SH power measured at QPM resonances allowed us to determine the relative strength of all quadratic nonlinearity tensor elements. Finally, we estimated the magnitude of the largest nonlinear coefficient, d_{31}, at the level of 1.3 pm/V. This result was validated by conducting a control experiment with a CBN crystal with known nonlinearity. This is the first quantitative measurement of nonlinear properties of a PMN-38PT crystal. While weaker than expected, the nonlinearity of the PMN-38PT material may still allow integration of piezoelectric and nonlinear functionalities in a single crystal. Consequently, our results could be also relevant for other tetragonal PT-relaxors.

Funding. National Natural Science Foundation of China (11904273, 11974196, 61675158); Research Start-up Program of Xidian University (10251180017); Yongjiang Scholar Foundation of Ningbo; Qatar National Research Fund (NPRP 12S-0205-190047).

Acknowledgment. ANU Centre for Advanced Microscopy (CAM).

Disclosures. The authors declare no conflicts of interest.

Data availability. Data underlying the results presented in this paper are not publicly available at this time but may be obtained from the authors upon reasonable request.

REFERENCES

1. S. Zhang and F. Li, J. Appl. Phys. **111**, 031301 (2012).
2. E. Sun and W. Cao, Prog. Mater. Sci. **65**, 124 (2014).
3. F. Li, D. Lin, Z. Chen, Z. Cheng, J. Wang, C. Li, Z. Xu, Q. Huang, X. Liao, and L. Q. Chen, Nat. Mater. **17**, 349 (2018).
4. C. Qiu, B. Wang, N. Zhang, S. Zhang, J. Liu, D. Walker, Y. Wang, H. Tian, T. R. Shrout, and Z. Xu, Nature **577**, 350 (2020).
5. Y. Lu, Z. Y. Cheng, Y. Barad, and Q. M. Zhang, J. Appl. Phys. **89**, 5075 (2001).
6. F. Wu, B. Yang, E. Sun, G. Liu, H. Tian, and W. Cao, J. Appl. Phys. **114**, 027021 (2013).
7. Y. Zhao, X. Liu, B. Li, Q. Hu, Y. Zhuang, X. Fu, P. Luan, W. Zhao, Y. Liu, and Z. Li, Ferroelectrics **542**, 112 (2019).
8. J. Midwinter and J. Warner, Br. J. Appl. Phys. **16**, 1135 (1965).
9. J. A. Armstrong, N. Bloembergen, J. Ducuing, and P. Pershan, Phys. Rev. **127**, 1918 (1962).
10. D. S. Hum and M. M. Fejer, C. R. Phys. **8**, 180 (2007).
11. S. Matsumoto, E. Lim, H. Hertz, and M. Fejer, Electron. Lett. **27**, 2040 (1991).
12. F. Li, L. Wang, L. Jin, Z. Xu, and S. Zhang, CrystEngComm **16**, 2892 (2014).
13. A. D. Ushakov, A. A. Esin, A. R. Akhmatkhanov, Q. Hu, X. Liu, Y. Zhao, X. Wei, and V. Ya. Shur, Appl. Phys. Lett. **113**, 112902 (2018).
14. X. Liu, Y. Zhao, Q. Hu, A. D. Ushakov, P. Luan, X. Fu, W. Zhao, Y. Zhuang, A. R. Akhmatkhanov, V. Ya. Shur, Y. Liu, Z. Li, X. Wei, and Z. Xu, J. Eur. Ceram. Soc. **40**, 2922 (2020).
15. P. Zelenovskiy, E. Greshnyakov, D. Chezganov, L. Gimadeeva, E. Vlasov, Q. Hu, X. Wei, and V. Shur, Crystals **9**, 65 (2019).
16. X. Chen, D. Liu, S. Liu, L. M. Mazur, X. Liu, X. Wei, Z. Xu, J. Wang, Y. Sheng, Z. Wei, and W. Krolikowski, Adv. Opt. Mater. **10**, 2102115 (2022).
17. X. Chen, P. Karpinski, V. Shvedov, K. Koynov, B. Wang, J. Trull, C. Cojocaru, W. Krolikowski, and Y. Sheng, Appl. Phys. Lett. **107**, 141102 (2015).
18. X. Chen, P. Karpinski, V. Shvedov, A. Boes, A. Mitchell, W. Krolikowski, and Y. Sheng, Opt. Lett. **41**, 2410 (2016).
19. T. Xu, K. Switkowski, X. Chen, S. Liu, K. Koynov, H. Yu, H. Zhang, J. Wang, Y. Sheng, and W. Krolikowski, Nat. Photonics **12**, 591 (2018).
20. S. Liu, K. Switkowski, C. Xu, J. Tian, B. Wang, P. Lu, W. Krolikowski, and Y. Sheng, Nat. Commun. **10**, 1 (2019).
21. L. M. Mazur, S. Liu, X. Chen, W. Krolikowski, and Y. Sheng, Laser Photonics Rev. **15**, 2100088 (2021).
22. S. Zhang, J. Luo, W. Hackenberger, and T. R. Shrout, J. Appl. Phys. **104**, 064106 (2008).
23. F. Li, L. Jin, Z. Xu, and Z. Guo, Rev. Sci. Instrum. **80**, 085106 (2009).
24. Y. Sheng, A. Best, H. J. Butt, W. Krolikowski, A. Arie, and K. Koynov, Opt. Express **18**, 16539 (2010).
25. J. Thomas, V. Hilbert, R. Geiss, T. Pertsch, A. Tünnermann, and S. Nolte, Laser Photonics Rev. **7**, L17 (2013).
26. M. M. Fejer, G. A. Magel, D. H. Jundt, and R. L. Byer, IEEE J. Quantum Electron. **28**, 2631 (1992).
27. A. Weiner, *Ultrafast Optics* (John Wiley & Sons, 2011), Vol. 72.
28. C. He, W. Ge, X. Zhao, H. Xu, H. Luo, and Z. Zhou, J. Appl. Phys. **100**, 113119 (2006).
29. A. Arie and N. Voloch, Laser Photonics Rev. **4**, 355 (2010).
30. S. Bancelin, S. Vigne, N. Hossain, M. Chaker, and F. Légar, Opt. Express **24**, 17497 (2016).
31. M. Eßer, M. Burianek, P. Held, J. Stade, S. Bulut, C. Wickleder, and M. Mühlberg, Cryst. Res. Technol. **38**, 457 (2003).